

## MODELLING OF RESISTIVE PULSE SENSING: FLEXIBLE METHODS FOR SUBMICRON PARTICLES

G. R. WILLMOTT<sup>1</sup> and B. G. SMITH<sup>2</sup>

(Received 19 March, 2012; revised 9 January, 2014; first published online 6 June 2014)

### Abstract

Nanopore science, the study of individual nanoscale pores within thin membranes, is a fast-growing field which presents numerous interesting problems for physicists and applied mathematicians. Nanopores are most commonly applied to resistive pulse sensing (RPS) of individual particles suspended in aqueous electrolyte. The form of a resistive pulse is dependent on an array of experimental variables, including electrolyte characteristics, electrophoretic and convective transport, and (especially) pore and particle geometry. The level of analysis required depends on the application, but any broadly useful approach should be simple and flexible, due to the requirement for high data throughput and variations between different experimental systems and specimens. Here we review analytic methods for interpreting RPS experiments for particles in the approximate range 100 nm to 1  $\mu\text{m}$ , focusing on calculation of resistance change as a function of the particle's position. We detail a recently developed semi-analytical model and compare the modelled electric field with finite element results. The model can also be used to calculate particle motion, so that the experimental current–time history can be reconstructed. This approach is useful for a wide range of pore and particle geometries, and includes consideration of entrance effects. Tunable elastomeric pores with truncated linear cone geometry are used as a model system.

2010 *Mathematics subject classification*: 70G99.

*Keywords and phrases*: nanopore, resistive pulse sensing, tunable pore.

### 1. Introduction

Nanopores—individual nanoscale holes in thin membranes—are simple geometric building blocks, which are likely to find many uses in nanoscience and nanotechnology. To date, they have usually been used for resistive pulse sensing (RPS,

<sup>1</sup>The MacDiarmid Institute for Advanced Materials and Nanotechnology, Callaghan Innovation, PO Box 31310, Lower Hutt 5040, New Zealand.

Present Address: Department of Physics, The University of Auckland, New Zealand;  
e-mail: [g.willmott@auckland.ac.nz](mailto:g.willmott@auckland.ac.nz).

<sup>2</sup>Callaghan Innovation, PO Box 2225, Auckland 1140, New Zealand;  
e-mail: [bryan.smith@callaghaninnovation.govt.nz](mailto:bryan.smith@callaghaninnovation.govt.nz).

© Australian Mathematical Society 2014, Serial-fee code 1446-1811/2014 \$16.00

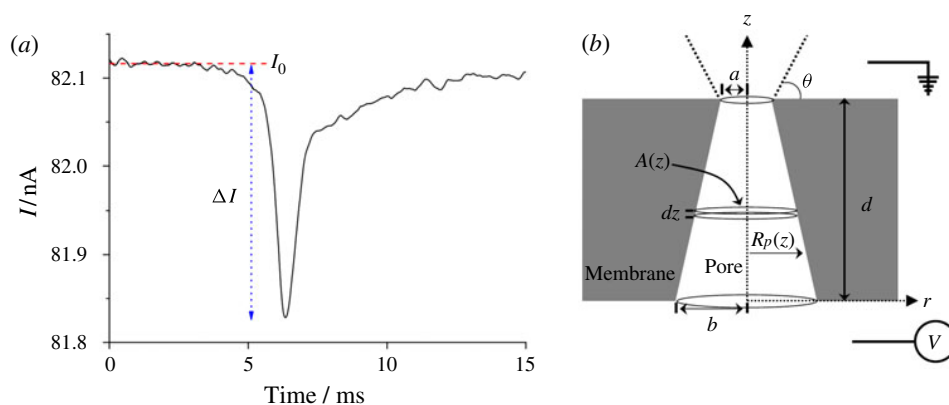


FIGURE 1. (a) An experimental resistive pulse event caused by a single 955 nm polystyrene sphere passing through a tunable elastomeric pore, filled and surrounded with 0.1 M electrolyte, with 0.12 V applied across the membrane. The pulse magnitude  $\Delta I$ , measured relative to the baseline current  $I_0$ , corresponds to a resistance magnitude  $\Delta R$ . Event asymmetry arises from the pore geometry. (b) A schematic section of a pore, with  $V$  applied across the membrane. Geometric parameters are defined in the text.

Figure 1(a)), in which pores are filled with and surrounded by aqueous electrolyte. When a potential  $V$  is applied across the membrane, an ionic current  $I_0$  flows between the electrodes, and if a particle then passes (or is driven) through the pore, there is a brief change in the pore resistance. This change, usually observed in experimental current–time histories, is known as a resistive pulse and has magnitude  $\Delta R$ . Extracting information about the particle from this resistive pulse presents a challenge for physicists and applied mathematicians.

Nanopores come in many shapes and sizes. Biological ion channels [4, 9, 10, 14, 32], silicon-based pores [3, 18, 20, 35, 60] and even thin carbon sheets [53] are used for single-molecule sensing, particularly of DNA. However, a wide range of nanopore research, and research problems, fall into the larger submicron range between single molecules and  $1 \mu\text{m}$  [36]. Many drug delivery technologies, viruses, synthetic beads, blood constituents, emulsions and bioparticles fall into this range. Corresponding nanopores can be made from large carbon nanotubes [28, 29], glass [2, 37, 57, 58, 63], polymers [26, 48, 52, 66] and elastomers [31, 36, 41, 42, 46, 47, 56, 61, 62, 67–71, 73]. When the size of the electrical double layer adjacent to surfaces (1–10 nm for typical electrolytes) is relatively small, the electrolyte can be considered to be homogeneous. This is known as the high salt limit.

The applied nature of nanopore science is self-evident in the research reported using these pores, which results in exciting and interdisciplinary experiments. However, nanopore experiments have often encouraged speculative interpretations based on qualitative observations of the resistive pulse sizes and shapes, or intuition. For quantitative interpretations of RPS, the size and shape of the resistive pulse should be understood on the basis of the corresponding experimental parameters. The range of interacting considerations, such as electrokinetics, fluid mechanics, rigid body

dynamics, electrolyte and surface chemistries, pore geometry, and so on—appears daunting when detailed analysis is required. On the other hand, real-world applications of pores often involve high particle throughput, requiring an efficient and flexible approach.

In this paper we discuss efforts to understand RPS in the submicron range using mathematical models with particular focus on modelling the size of the pulse. Kozak et al. [36] and Qin et al. [43] have recently compiled good summaries of similar material, but whereas past workers have usually attempted to find  $\Delta R$  for simple particle and pore geometries (especially a sphere in a long cylinder), we emphasize methods where the resistance change can be calculated as a function of particle position, and the pore and particle geometries are not strongly restricted. This is important for RPS using conical pores for detection of clusters [71], or when a particle is near the entrance of a pore, for example. We then discuss particle transport, which is required to reconstruct the full shape of a current–time history, and determine its duration. The transport and resistance calculations can be considered independently, when an instantaneous current measurement is independent of particle motion, for example, the quasi-static case. A semi-analytic model for RPS has recently been developed using these principles [42, 61, 62, 70–72], and we compare this model with new finite element results, addressing its strengths and weaknesses.

Figure 1(b) introduces the generic geometry and variables used in this paper. Although the figure shows a truncated linear cone, much of the discussion applies to any pore of radius  $R_P(z)$  (when sections are circular and centred on the  $z$ -axis), or more generally of sectional area  $A(z)$ . We refer to two specific geometries: firstly, the truncated linear cone which has opening radii  $a$  and  $b$  in a membrane of thickness  $d$ ; and secondly, a cylinder of radius  $a_0$ . When a spherical particle is present, it has radius  $a'$ . The truncated linear cone geometry is relevant to tunable elastomeric pores [31, 36, 41, 42, 46, 47, 56, 61, 62, 67–71, 73], which is our model experimental system. Tunable pores are made by puncturing an elastomeric membrane with a sharpened tip, producing a conical shape pore [56, 67]. The membrane can be reversibly actuated on macroscopic scales in order to stretch and relax the micro- to nanoscale conical pore geometry [68], so that the ionic current passing through the pore varies by at least an order of magnitude [69]. Although sensing of single-molecule DNA has been reported [56], tunable pores are typically used to investigate particles from around 70 nm up to approximately 1  $\mu\text{m}$ . Due to membrane stretching, individual pore specimens can measure particles over a range of sizes, including multimodal particle size distributions [46, 67].

## 2. The electric field and current through a pore

**2.1. Models for an open pore** The electric field distribution is an important parameter in nanopore experiments, determining the resistance of an open pore (therefore, the background current  $I_0$ ) and the change in resistance when a particle is present within the pore, so that a resistive pulse of magnitude  $\Delta R$  is observed. For

efficient, flexible analysis of RPS with nanopores, it has proved useful to consider the analytic electric field  $\mathbf{E}$ , as governed by the Laplace equation in electrostatics,

$$\nabla^2 v = 0, \quad (2.1)$$

where the electric potential  $v$  is a function of position, and Ohm's law gives  $\mathbf{E} = -\nabla v = -I\nabla R$  where  $I$  and  $R$  are current and resistance, respectively. Here the electrolyte is assumed to be homogeneous, which is effectively the case in the high salt limit. Equation (2.1) can be solved for a specific nanopore geometry of interest, noting that the pore membrane is usually insulating. The electrodes used to apply the fixed voltage  $V$  can be important for this calculation. Here, we assume that a semi-infinite half-space exists above and below the membrane, so that the voltage drop between electrodes occurs entirely within the pore and its immediate surroundings. This assumption is reasonable when the length scales associated with the pore are small compared to the electrode surface areas, and the distance from each electrode to the pore. For tunable pores, this condition is satisfied: the electrodes are wires, several millimetres long and approximately 1 mm in diameter, located several millimetres away from the pore, whereas the larger pore opening diameter is approximately 50  $\mu\text{m}$ . Polarization potential at the electrodes [30, 34, 55] is assumed negligible.

Exact analytic solutions of the Laplace equation have been used for calculation of the electric field in and around a pore for some specific geometries. Beyond the simplest case of a long cylinder [3, 59], Kowalczyk et al. [35, 72] recently found the electric field for a double-hyperboloid geometry, appropriate for their hourglass-shaped silicon-based nanopores. However, pores with various cross-sections (usually near-conical) often arise from manufacturing processes such as laser heating [75], track etching [26] and in glass [2, 38, 58]. Mechanically punctured tunable pores are also conical [62, 70, 73], and moreover their geometry varies when stretch is applied to the membrane. The exact solutions available are not applicable for most pore types, and they do not work when a particle is near the entrance of a pore.

A common method for more general geometry is to find the incremental resistance of the pore across a slice of thickness  $dz$  perpendicular to the pore's central  $z$ -axis (Figure 1(b)). Using this series resistance methodology (often applied to wire conductors) with electrolyte resistivity  $\rho$ , the incremental resistance is

$$R \approx \rho \int \frac{dz}{A(z)}, \quad (2.2)$$

where we use approximate equality to indicate a mathematical model of a physical system. This method has the clear benefit that the pore shape defined by  $A(z)$  is not restricted to any particular geometry, although there is an additional assumption that  $A(z)$  is slowly varying with respect to  $z$ . A consequence of this assumption is that the radial component of the electric field is zero, or insignificant compared to the vertical component. Pore slices taken perpendicular to the  $z$ -axis are equipotential surfaces, and the electric field is the same at any particular value of  $z$ . Resistance calculations converge with full solutions to Laplace's equation, such as the hyperboloid model

[72], when the radius is slowly varying. This approach has been proved useful for studying open-pore conductance [26, 33, 35, 40]. Use of equation (2.2) can yield simple functional forms, for example, if the resistance between the ends of a pore is  $R_{in}$ , then the result for a truncated linear conical pore of length  $d$  with opening radii  $a$  and  $b$  is

$$R_{in,cone} \approx \frac{\rho d}{\pi ab},$$

an expression used in various studies [26, 58, 62, 70].

The electric field near the ends of the pore (entrance effects) is especially important when the membrane is thin, when the pulse shape is of interest, or when the constriction is near one-membrane surface (for example, conical pores). Model pore geometries typically include an abrupt transition at the pore entrance. When modelling the resistance change between the pore entrance and an electrode ( $R_{out}$ ), there is a known solution for a circular disc entrance (radius  $a$ ) and a semi-infinite half-space [23],

$$R_{in,disc} \approx \frac{\rho}{4a}. \quad (2.3)$$

The resistance drop from a circular pore opening to an adjacent half-space is equivalent to  $R_{in,disc}$ , when there is an equipotential across the surface of the opening, as is the case when using equation (2.2) to find  $R_{in}$ . Therefore,  $R_{in,disc}$  can be added to  $R_{in}$  to give a piecewise solution for  $\mathbf{E}$ , which is continuous between the ends of the pore and the pore interior. This method has often been used in pore analyses [17, 24, 28, 58, 73], and for the special case of the truncated conical pore, the total resistance with no particle present is

$$R_{cone} \approx \frac{\rho}{\pi ab} \left[ d + \frac{\pi}{4}(a + b) \right],$$

where a value of 0.8 is sometimes used in place of the factor  $\pi/4 \approx 0.785$ .

The resistance between a hemispherical surface and the infinite half-space can also be calculated analytically [46]. When the hemisphere is an equipotential of radius equal to the pore opening, the calculated resistance ( $\rho/2\pi a$ ) can be treated as a lower bound for  $R_{out}$ , because resistance between the disc and the hemisphere has been omitted. The hyperboloid geometry used by Kowalczyk et al. [35] generated an equipotential surface protruding from the pore entrance, so that  $R_{out}$  was bounded between the results for the disc as in equation (2.3) and the hemisphere.

**2.2. Addition of an insulating particle** Once the open-pore resistance is known, the change in resistance when a particle is added can be determined. DeBlois et al. [15] described several methods for this calculation, starting with an approach (attributed to Maxwell) in which the fractional resistance change is equal to the ratio of the particle and pore volumes. For a spherical particle of radius  $a'$  within a cylindrical pore of radius  $a_0$ , the resistance change is

$$\Delta R_{Maxwell} \approx \frac{2\rho a'^3}{\pi a_0^4}. \quad (2.4)$$

This expression is valid when  $a' \ll a_0$ , and when the pore is long enough that end effects are not important. Note that there is no dependence on the pore length in equation (2.4), and no provision for specification of the pore geometry local to the particle. It follows that the volumetric approach is unsuitable when  $R_p(z)$  is not constant. However, the principle that  $\Delta R$  is proportional to the particle volume is observed more widely. For example, it is the basis of a method for sizing particles using a conical pore, as long as the particle remains small relative to the pore [62].

Using equation (2.2), Gregg and Steidley [21] calculated  $\Delta R$  for a sphere, again assuming that  $a' \ll d$  and  $R_p(z)$  is constant, but allowing for relatively large particles. For this method, the area of the pore increment excludes the insulated area obstructed by the particle. The closed analytic solution is

$$\Delta R_{GS} \approx \frac{2\rho}{\pi a_0} \left[ \frac{\sin^{-1}(a'/a_0)}{(1 - (a'/a_0)^2)^{1/2}} - \frac{a'}{a_0} \right]. \quad (2.5)$$

Although this equation describes a specific geometry, a major advantage of Gregg and Steidley's method is that it can be applied to any particle and pore geometry. For example, Heins et al. [26] were able to obtain a similar analytic result for a truncated linear cone, albeit without consideration of end effects. Equation (2.5) gives good agreement with experiments for large spheres [15], because the curvature ensures relatively slow variation of the conducting cross-section along the  $z$ -axis. This condition is similar to the assumption noted above when using equation (2.2) to calculate the open-pore resistance in the noncylindrical case. However, the assumption that the electric field is uniform across the pore width gives rise to two practical drawbacks. Firstly, there is no accounting for differences between on- and off-axis particles. Secondly,  $\Delta R_{GS}$  is a lower bound for the total resistance, because nonuniformity in the field will always increase the overall resistance. In the limit  $a' \ll a_0$ ,  $\Delta R_{GS}$  is a factor of two-thirds smaller than  $\Delta R_{Maxwell}$  [15], so calculated results can be multiplied by an empirical correction factor of 1.5 when modelling small particles.

DeBlois et al. [15] further suggested using the solution to the Laplace equation for a sphere in a uniform field, with the assumption that the bulging electric field lines did not extend far beyond the edges of the pore. The resulting expression agrees with Maxwell's solution in the small sphere limit, and with Gregg and Steidley's as the particle size approaches the pore size. Numerical methods were also used to solve the problem of a sphere within a cylinder [54], prompting DeBlois et al. to summarize [16] that the resistance change can be written as

$$\Delta R_{Num} \approx \frac{2\rho a'^3}{\pi a_0^4} S\left(\frac{a'}{a_0}\right), \quad (2.6)$$

where, if the function  $S$  is

$$S\left(\frac{a'}{a_0}\right) = \frac{1}{1 - 0.8(a'/a_0)^3},$$

then the variation with the numerically calculated values does not exceed 1% for  $a'/a_0 \leq 0.8$ . The simple form of equation (2.6) works well for cylindrical pores, where the pore length is larger than the pore width, and the particle size is much smaller than the pore size. However, neither does it allow consideration of variable pore and particle geometry nor of entrance effects. To account for different particle geometries, an arbitrary shape factor can be added to equation (2.6) [36]. Qin et al. [43] have modelled RPS for ellipsoidal particles, while also considering entrance effects. Using cylindrical pores, Qin et al. and Berge et al. [5] also modelled RPS for off-axis particles. The hydrodynamic drag on a particle is altered when the particle is off-axis, or large in comparison with the pore width [25].

The semi-analytic method we have recently used [42, 61, 62, 70–72] applies equation (2.2) with the particle area excluded from the integral, as used for equation (2.5). The main advantage of this method is that it can be applied to any pore and particle geometry, as long as it is slowly varying along the pore length. Consideration of geometry is paramount, because it is a first-order effect—note the dependence of  $\Delta R$  on geometric parameters in equations (2.4)–(2.6). The geometric flexibility enables the resistance change to be calculated with the particle at any position along the length of the pore, and at any orientation. For smooth functions, the calculation of  $R_{\text{in}}$  using equation (2.2) can be achieved efficiently using a standard numerical solver (for example, the Matlab quad function). As mentioned above, the important disadvantages are: (i) forced electric field uniformity across the pore width, so that the particle should be assumed to lie near the central axis of the pore; (ii) the need to consistently use the empirical correction factor of 1.5 when the particle size is much smaller than the pore width, as is usually the case for RPS. Therefore, the method is best applied to comparative studies of similar experiments, an approach successfully applied to particle sizing [28, 58, 62] and resistive pulse asymmetry [58, 70] rather than calculation of absolute values.

To complete the description of the semi-analytic method, we revisit entrance effects. Although the resistance between the pore opening and a half-space is known, calculation of the electric field in the half-space with a particle present is not trivial. It is, therefore, difficult to analytically find the correction to the total resistance, when a particle is close to the end of the pore. One way of estimating this effect is to create an artificial cone within the half-space (Figure 1(b)). The pitch of this cone can be set to  $\tan \theta = 0.8$ , so that the resistance between the pore and the half-space calculated using equation (2.2) agrees with the analytic value in equation (2.3). Any particle in the half-space is then treated as a particle within a constriction defined by the artificial cone, so that  $R_{\text{out}}$  can be numerically calculated in the same way as  $R_{\text{in}}$ , using equation (2.2). This approach is clearly inaccurate off-axis (for example, outside the artificial cone) and a comparison with finite element solutions is presented below. However, entrance effects have seldom been analytically addressed for RPS, despite their importance, which is demonstrated in Figure 2 [70]. Here, the maximum deviation from the baseline current (which defines  $\Delta R$ ) occurs when the particle protrudes from the pore into the half-space.

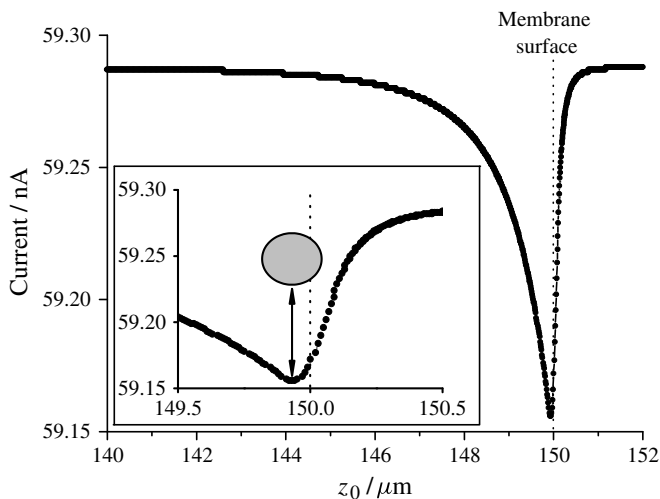


FIGURE 2. A current simulation (reproduced from [70]), plotted against the  $z_0$ -axis position of the centre of a sphere ( $z_0$ ) using the semi-analytic model with truncated linear cone geometry. Here  $a' = 110$  nm,  $a = 450$  nm,  $b = 20$   $\mu\text{m}$ ,  $d = 150$   $\mu\text{m}$  and 0.3 V was applied using electrolyte of resistivity  $\rho = 0.86$   $\Omega\text{m}$ . Inset: A magnification near the membrane surface, with the sphere (depicted at the scale of the horizontal axis) located at the value of  $z_0$  where the current is minimized.

### 3. Comparison with finite element results

The finite element method (FEM) has been used to calculate the electric field in a pore for comparison with the semi-analytic modelling approach outlined above. The Laplace equation was solved numerically for pores of a specific geometry, assuming that the electrolyte is homogeneous, and that the pore and particle are insulators. The electric field normal to these insulating surfaces is zero, and the other boundary condition is the applied potential difference  $V$  far from the pore on either side of the membrane. Calculations used Comsol Multiphysics 3.3 with a triangular mesh and  $\sim 60\,000$  degrees of freedom. A finite radius of curvature was applied at the sharp lip of the pore to avoid numerical instability. Results are shown in Figure 3.

Comparison between the semi-analytic and FEM results for the open-pore conductance is shown in Figure 3(a). On-axis, the two methods differ by less than 35% everywhere, with the most significant deviations ( $>10\%$ ) only occurring in the region  $149.8 \leq z \leq 151.5$   $\mu\text{m}$  at the discontinuous pore entrance. FEM confirms that  $E_r \ll E_z$  for the typical tunable pore geometry used. Even the largest values of  $E_r$  (near the cone edge) only reach a reasonable fraction of  $E_z$  very close to the pore entrance. Previously, finite element simulations of electric fields have been carried out for conical pores [38, 39, 58], and for a DNA-sensing pore [27], for example. For conical pores, these results qualitatively agree with our work.

Figure 3(a) also shows the variation in  $E_z$  across the width of the pore as a function of  $z$ . When using the semi-analytic method, there is no variation. The FEM results

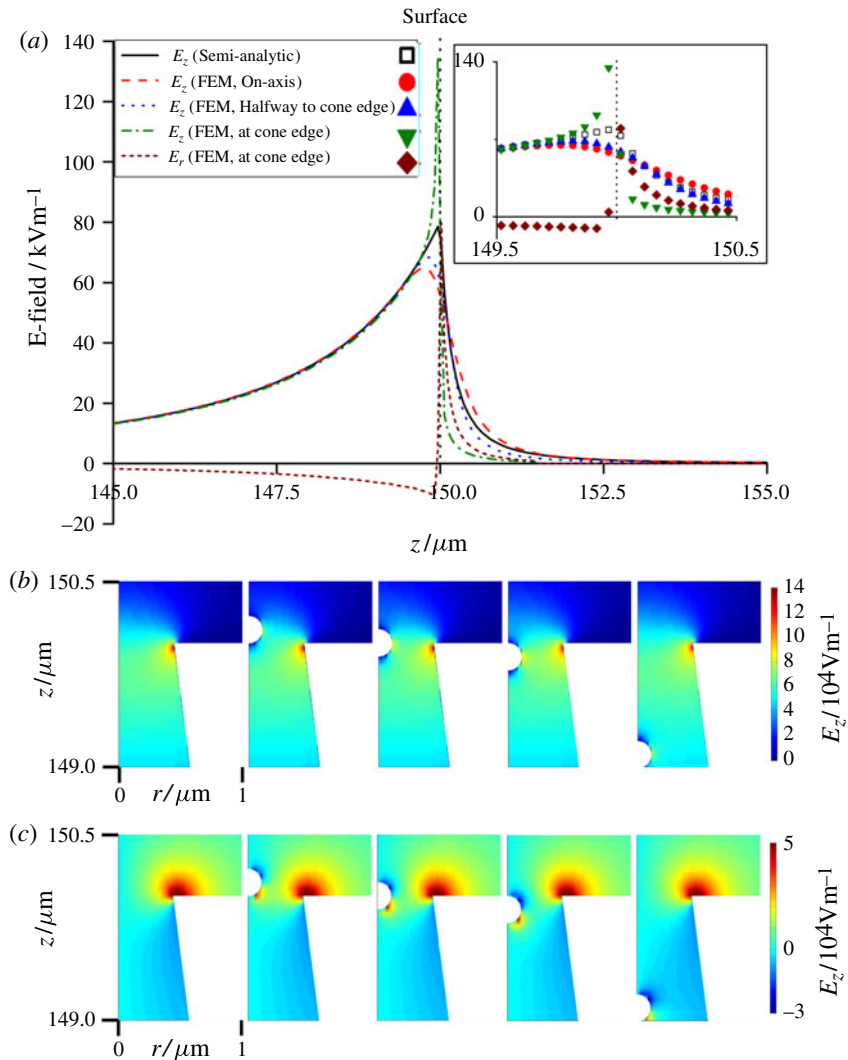


FIGURE 3. Comparison of finite element method results with the semi-analytic method for the electric field in a truncated conical pore with  $a = 450 \text{ nm}$ ,  $b = 20 \mu\text{m}$  and  $d = 150 \mu\text{m}$ , with  $0.3 \text{ V}$  applied across the membrane. (a) Plot of electric field components (as shown by Willmott and Smith [72]), but with greater spatial resolution), including variation of  $E_z$  across three radial positions. In the half-spaces, the cone edge is defined by the artificial cone. Inset: a magnification of the same plot near the membrane surface, with individual mesh points plotted. (b) and (c) Intensity plots of the axial and radial electric fields, respectively, in a radial slice through the pore, where white areas indicate insulating material. In each case, the five images correspond (from left to right) to: (i) an open pore, and with the sphere centre positioned; (ii) one radius above the surface; (iii) at the surface; (iv) one radius below the surface; (v) one pore diameter below the surface.

reveal that through most of the pore, the field half way between the central axis and the edge of the pore is slightly smaller than on-axis, and the field at the pore edge is smaller still. At the pore entrance, the electric field becomes concentrated near the sharp lip of the pore, so that the field at the edge is much greater than on-axis. As expected, the artificial cone construction in the half-space is only suitable for describing the on-axis field, and the off-axis values for the semi-analytic and FEM results do not agree well. The radial field intensity plot (Figure 3(c)) demonstrates that the radial field is significant near the pore lip, and on either side of a sphere within the pore.

#### 4. Particle transport

For full reconstruction of a current–time resistive pulse, there remains the challenge of combining resistance calculations with nano- and microfluidic transport properties. By calculating the particle position as a function of time, the experimental pulse can be simulated under the assumption that the electric field is quasi-static. The starting point for determining the transport properties of a particle within a micro- or nanopore is the Nernst–Planck equation, which simply sums contributions to the particle flux  $\mathbf{J}$ , that is, the number of particles passing through a unit area per unit time. For example, taking the summation of (from left to right) diffusion, electrophoresis, electro-osmosis and pressure-driven transport, we have

$$\mathbf{J} \approx \mathbf{J}_{\text{diff}} + \mathbf{J}_{\text{eph}} + \mathbf{J}_{\text{eo}} + \mathbf{J}_{\text{pd}}.$$

Further mechanisms, for example, magnetophoresis [71] can be added in some circumstances. Together, electrophoresis and electro-osmosis comprise electrokinetic transport, while electro-osmotic and pressure-driven mechanisms are convective, because transport of particles is due to the motion of fluid rather than the motion of particles relative to the fluid.

Considering first the motion of a relatively large particle within homogeneous electrolyte, we can discard diffusive transport, because there is no ionic concentration gradient. The sum of electrokinetic fluxes is

$$\mathbf{J}_{\text{eph}} + \mathbf{J}_{\text{eo}} \approx \frac{C\epsilon}{\eta} (\zeta_{\text{particle}} - \zeta_{\text{pore}}) \mathbf{E}. \quad (4.1)$$

Here,  $C$  is the particle concentration,  $\zeta$  refers to the zeta potential of the subscripted surface, and  $\eta$ ,  $\epsilon$  are the viscosity and absolute permittivity of the electrolyte, respectively. As written, these terms apply when the extent of the electrical double layers at the particle and pore surfaces is small in comparison with the particle size (for  $\mathbf{J}_{\text{eph}}$ ) and pore width (for  $\mathbf{J}_{\text{eo}}$ ), respectively. Construction of electrical double layers is well studied [34, 45, 51], and the characteristic double layer thickness is unlikely to exceed 10 nm for typical electrolytes [22], so equation (4.1) is applicable for sensing of particles in the 100 nm to 1  $\mu\text{m}$  range. In this range, it is interesting that the electrophoretic mobility of a spherical particle is proportional to  $\zeta_{\text{particle}}$ , implying that  $\zeta_{\text{particle}}$  is proportional to  $\sigma a'$ , where  $\sigma$  is the charge per surface area, so  $\zeta_{\text{particle}}$  scales

in proportion to  $a'$ . The electro-osmotic flow velocity in equation (4.1) is independent of radial position (plug flow), and is derived for a cylindrical tube. However, this expression can be used for long, thin tubes [34] and is more generally applicable in many cases [12, 50]. The expression in equation (4.1) can also be applied to the semi-analytic resistive pulse model, because  $\mathbf{E}$  has been determined as described above. Methods such as dynamic light scattering (for particles) [6] and electro-osmotic flow velocity measurements (for pore walls) [19, 34] can be used to determine zeta potentials.

If the pressure across the membrane  $\Delta P$  is known, then the pressure-driven term  $\mathbf{J}_{pd}$  can be determined using Stokes's equation for laminar flow. The Hagen–Poiseuille result for a cylinder can be applied to a general cylindrical increment of length  $dz$  and radius  $R_p(z)$  (Figure 1(b)), so that

$$\frac{dP}{dz} \approx \frac{8\eta Q}{\pi(R_p(z))^4}, \quad (4.2)$$

where  $dP$  and  $Q = C J_{pd,z}$  are the pressure drop and the flow rate across the increment, respectively. Note the dependence of flow rate on the fourth power of pore width; when using tunable pores, for example, a small microfluidic pressure head can dominate the flow of particles through a micron-sized pore, whereas electrokinetic effects are significant and compete with pressure for pore sizes approaching 100 nm [61].

Equation (4.2) can be integrated along the length of any pore with circular cross-sections to determine the flow rate if the overall pressure drop is known. As with the electric field, entrance effects should be considered, and in this case Sampson's solution for the flow rate through a thin circular orifice applies [49]. This solution has been validated numerically for tubes of nonzero [13] and semi-infinite [64] length.

The model given in equation (4.2) also forms the basis for the semi-analytical model used in recent work involving particle transport [61, 70, 71], with entrance effects included. Figure 4 demonstrates use of the model [71]. Firstly, the modelled pore geometry and applied pressure were calibrated, so that the baseline current, pulse height, duration and asymmetry were consistent with average resistive pulses caused by standard polystyrene particles. When different superparamagnetic particles were used with the same pore, the modelled events agree well with experimental pulse heights and shapes. Moreover, clustered particles can be identified and their pulses reproduced using this model. As with the electric field, an artificial cone is used to estimate the on-axis flow rate in the half-space. For our model geometry of a truncated linear cone, the analytical result is [37, 47, 61]

$$\Delta P \approx Q \left[ \frac{8\eta d}{3\pi} \frac{(a^{-3} - b^{-3})}{(b - a)} + \frac{3\eta}{2} (a^{-3} + b^{-3}) \right].$$

Pressure-driven flow is useful for determining particle concentration, when  $\mathbf{J}_{pd}$  dominates, so that the rate of resistive pulses is simply proportional to  $C$  [47, 73, 74]. Lan et al. [37] recently analysed and simulated pressure-driven flow through a nanopore in some detail, while precise control of pressure could allow determination of particle mobility and, therefore, zeta potential [61].

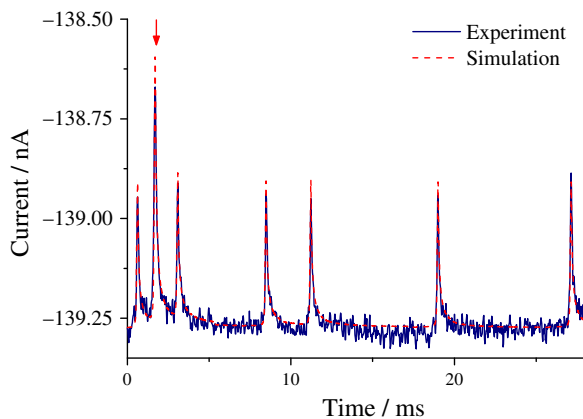


FIGURE 4. Part of an experimental current history (reproduced from [71]) for  $1\ \mu\text{m}$  superparamagnetic beads passing through a tunable pore, some of which are clustered due to application of a magnetic field. The semi-analytic model has earlier been calibrated using standard particles. Simulated traces are overlaid on the experimental data, aligned so that the baseline currents and peak times coincide. The peak denoted by the red arrow corresponds to a simulation of a dimer passing through the same pore.

So far, all our detailed considerations of resistive pulse height and particle transport have assumed that the electrolyte is homogeneous, which is a practical assumption in the high salt limit. However, the rigour of the analysis could be improved by including ionic species distributions, the hydrodynamics of the double layers, and formation of an asymmetric charge cloud around the particle. Detailed consideration of ionic transport should account for co-dependency between local electrolyte resistivity and the electric field, because electrophoretic motion of ions in the field will alter the resistivity. When a steady state is reached, the net motion of ions will determine the current passing through the pore. An additional level of complication is introduced if the particle is moving fast enough that the steady state does not dominate, so that dynamic effects are important. For meaningful detailed modelling of ionic species near the pore wall, the surface charge must be well known.

To obtain steady-state solutions, Poisson–Nernst–Planck (PNP) theory is usually used [38, 65], as described by Rice and Whitehead [45] for the base case of an open, cylindrical pore with no radial variation of the electric field. In PNP theory, a spatial density of each ionic species  $i$  is considered. Ions near a charged surface, such as pore walls, follow Poisson’s equation in electrostatics, which allows the double layer to be defined. The Nernst–Planck equation is then applied to determine the current density carried by each species  $\mathbf{J}_i$ . For example, considering only diffusion and electrophoresis,

$$\mathbf{J}_i \approx -D_i \nabla C_i + \frac{z_i e}{k_B T} D_i C_i \mathbf{E},$$

where  $D_i$  is the diffusion coefficient,  $C_i$  is concentration,  $z_i e$  is the charge of an ion,  $k_B$  is Boltzmann’s constant and  $T$  is temperature. Lan et al. [38] recently presented

a hybrid approach, in which a finite element simulation of the electric field and ion fluxes was performed simultaneously with a simple dynamic calculation for the nanoparticle motion. For extending PNP theory to pores with nontrivial geometries and distributions of surface and ionic charge, recent work concerning small, solid-state pores of reasonably well-defined geometry is instructive [1, 7, 8, 11, 44]. Specific distributions of surface charge give rise to diode-like behaviour of the ionic current, which is also observed experimentally. Pressure-driven flow is not significant in such work due to pore size.

## 5. Conclusions

Although nanopore-based RPS processes have been well studied, development of practical methods for experimental analysis remains a challenge. For many applications, high throughput is an important consideration. The requirement for fast data analysis introduces restrictions on the processing time available, and possibly the amount of information available from a digitally sampled signal. Different levels of details are required for the analysis of different experiments. With these considerations in mind, flexible analysis methods that address the most obvious metrics are appealing. In this article, as in the development of our semi-analytic model, we have emphasized high utility analytic methods that go beyond the simplest models.

There remain some interesting questions for submicron RPS, particularly regarding hydrodynamic transport. Particles entering a pore will tend to be flow-focused along the central pore axis, and aspherical particles should also be preferentially aligned with respect to this axis. However, the extent to which this is realized in comparison with kinetics, steric interactions and Brownian motion is often unclear in experiments. For off-axis particles, or spheres which are large relative to the velocity profile across the pore, corrections to the hydrodynamic drag can be considered. Another interesting recent observation is that aggregated particles tend to become slightly separated in the pore constriction [71], suggesting the presence of relatively strong hydrodynamic forces. These may also have an interesting effect on soft particles, such as emulsions.

## Acknowledgement

The authors are supported by New Zealand's Ministry for Science and Innovation (NERF contract C08X0806).

## References

- [1] M. Ali, P. Ramirez, S. Mafé, R. Neumann and W. Ensinger, "A pH-tunable nanofluidic diode with a broad range of rectifying properties", *ACS Nano* **3** (2009) 603–608; doi:10.1021/nn900039f.
- [2] R. An, J. D. Uram, E. C. Yusko, K. Ke, M. Mayer and A. J. Hunt, "Ultrafast laser fabrication of submicrometer pores in borosilicate glass", *Optics Letters* **33** (2008) 1153–1155; doi:10.1364/OL.33.001153.
- [3] L. Bacri, A. G. Oukhaled, B. Schiedt, G. Patriarche, E. Bourhis, J. Gierak, J. Pelta and L. Auvray, "Dynamics of colloids in single solid-state nanopores", *J. Phys. Chem. B* **115** (2011) 2890–2898; doi:10.1021/jp200326w.

- [4] S. Benner, R. J. A. Chen, N. A. Wilson, R. Abu-Shumays, N. Hurt, K. R. Lieberman, D. W. Deamer, W. B. Dunbar and M. Akeson, "Sequence-specific detection of individual DNA polymerase complexes in real time using a nanopore", *Nature Nanotech.* **2** (2007) 718–724; doi:10.1038/nnano.2007.344.
- [5] L. I. Berge, T. Jossang and J. Feder, "Off-axis response for particles passing through long apertures in Coulter-type counters", *Meas. Sci. Technol.* **1** (1990) 471–474; doi:10.1088/0957-0233/1/6/001.
- [6] S. K. Brar, "Measurement of nanoparticles by light-scattering techniques", *Trends Anal. Chem.* **30** (2011) 4–17; doi:10.1016/j.trac.2010.08.008.
- [7] J. Cervera, A. Alcaraz, B. Schiedt, R. Neumann and P. Ramirez, "Asymmetric selectivity of synthetic conical nanopores probed by reversal potential measurements", *J. Phys. Chem. C* **111** (2007) 12265–12273; doi:10.1021/jp071884c.
- [8] J. Cervera, P. Ramirez, S. Mafé and P. Stroeve, "Asymmetric nanopore rectification for ion pumping, electrical power generation, and information processing applications", *Electrochimica Acta* **56** (2011) 4504–4511; doi:10.1016/j.electacta.2011.02.056.
- [9] J. Clarke, H.-C. Wu, L. Jayasinghe, A. Patel, S. Reid and H. Bayley, "Continuous base identification for single-molecule nanopore DNA sequencing", *Nature Nanotech.* **4** (2009) 265–270; doi:10.1038/nnano.2009.12.
- [10] S. L. Cockcroft, J. Chu, M. Amarin and M. R. Ghadiri, "A single-molecule nanopore device detects DNA polymerase activity with single-nucleotide resolution", *J. Am. Chem. Soc.* **130** (2008) 818–820; doi:10.1021/ja077082c.
- [11] D. Constantin and Z. S. Siwy, "Poisson–Nernst–Planck model of ion current rectification through a nanofluidic diode", *Phys. Rev. E* **76** (2007) 041202; doi:10.1103/PhysRevE.76.041202.
- [12] E. B. Cummings, S. K. Griffiths, R. H. Nilson and P. H. Paul, "Conditions for similitude between the fluid velocity and electric field in electroosmotic flow", *Anal. Chem.* **72** (2000) 2526–2532; doi:10.1021/ac991165x.
- [13] Z. Dagan, S. Weinbaum and R. Pfeffer, "An infinite-series solution for the creeping motion through an orifice of finite length", *J. Fluid Mech.* **115** (1982) 505–523; doi:10.1017/S0022112082000883.
- [14] D. W. Deamer and D. Branton, "Characterization of nucleic acids by nanopore analysis", *Acc. Chem. Res.* **35** (2002) 817–825; doi:10.1021/ar000138m.
- [15] R. W. DeBlois and C. P. Bean, "Counting and sizing of submicron particles by the resistive pulse technique", *Rev. Sci. Instrum.* **41** (1970) 909–916; doi:10.1063/1.1684724.
- [16] R. W. DeBlois, C. P. Bean and R. K. A. Wesley, "Electrokinetic measurements with submicron particles and pores by the resistive pulse technique", *J. Colloid. Interf. Sci.* **61** (1977) 323–335; doi:10.1016/0021-9797(77)90395-2.
- [17] R. W. DeBlois and R. K. A. Wesley, "Sizes and concentrations of several type C oncornaviruses and bacteriophage T2 by the resistive-pulse technique", *J. Virology* **23** (1977) 227–233.
- [18] C. Dekker, "Solid-state nanopores", *Nature Nanotech.* **2** (2007) 209–215; doi:10.1038/nnano.2007.27.
- [19] S. Devasenathipathy and J. G. Santiago, *Electrokinetic flow diagnostics, in micro- and nano-scale diagnostic techniques* (Springer-Verlag, New York, 2005).
- [20] M. Firnkies, D. Pedone, J. Knezevic, M. Döblinger and U. Rant, "Electrically facilitated translocations of proteins through silicon nitride nanopores: Conjoint and competitive action of diffusion, electrophoresis, and electroosmosis", *Nano Lett.* **10** (2010) 2162–2167; doi:10.1021/nl100861c.
- [21] E. C. Gregg and K. D. Steidley, "Electrical counting and sizing of mammalian cells in suspension", *Biophys. J.* **5** (1965) 393–405; doi:10.1016/S0006-3495(65)86724-8.
- [22] P. D. Grossman, *Capillary electrophoresis* (Academic Press, San Diego, CA, 1992).
- [23] J. E. Hall, "Access resistance of a small circular pore", *J. Gen. Physiol.* **66** (1975) 531–532; doi:10.1085/jgp.66.4.531.
- [24] A. Han, G. Schürmann, G. Mondin, R. A. Bitterli, N. G. Hegelbach, N. F. de Rooij and U. Staufer, "Sensing protein molecules using nanofabricated pores", *Appl. Phys. Lett.* **88** (2006) 093901; doi:10.1063/1.2180868.

- [25] J. Happel and H. Brenner, *Low Reynolds number hydrodynamics* (Noordhoff International, Leiden, The Netherlands, 1973); doi:10.1007/978-94-009-8352-6.
- [26] E. A. Heins, Z. S. Siwy, L. A. Baker and C. R. Martin, "Detecting single porphyrin molecules in a conically shaped synthetic nanopore", *Nano Lett.* **5** (2005) 1824–1829; doi:10.1021/nl050925i.
- [27] J. B. Heng, A. Aksimentiev, C. Ho, P. Marks, Y. V. Grinkova, S. Sligar, K. Schulten and G. Timp, "Stretching DNA using the electric field in a synthetic nanopore", *Nano Lett.* **5** (2005) 1883–1888; doi:10.1021/nl0510816.
- [28] T. Ito, L. Sun, M. A. Bevan and R. M. Crooks, "Comparison of nanoparticle size and electrophoretic mobility measurements using a carbon-nanotube-based Coulter counter, dynamic light scattering, transmission electron microscopy, and phase analysis light scattering", *Langmuir* **20** (2004) 6940–6945; doi:10.1021/la049524t.
- [29] T. Ito, L. Sun and R. M. Crooks, "Simultaneous determination of the size and surface charge of individual nanoparticles using a carbon nanotube-based Coulter counter", *Anal. Chem.* **75** (2003) 2399–2406; doi:10.1021/ac034072v.
- [30] A. V. Jagtiani, J. Carletta and J. Zhe, "A microfluidic multichannel resistive pulse sensor using frequency division multiplexing for high throughput counting of micro particles", *J. Micromech. Microeng.* **21** (2011) 065004; doi:10.1088/0960-1317/21/6/065004.
- [31] M. L. Jansen, G. R. Willmott, I. Hoek and W. M. Arnold, "Fast piezoelectric actuation of an elastomeric micropore", *Measurement* **46** (2013) 3560–3567; doi:10.1016/j.measurement.2013.05.023.
- [32] J. J. Kasianowicz, E. Brandin, D. Branton and D. W. Deamer, "Characterization of individual polynucleotide molecules using a membrane channel", *Proc. Natl. Acad. Sci. USA* **93** (1996) 13770–13773; doi:10.1073/pnas.93.24.13770.
- [33] M. J. Kim, M. Wanunu, D. C. Bell and A. Meller, "Rapid fabrication of uniformly sized nanopores and nanopore arrays for parallel DNA analysis", *Adv. Mater.* **18** (2006) 3149–3153; doi:10.1002/adma.200601191.
- [34] B. J. Kirby and E. F. Hasselbrink Jr, "Zeta potential of microfluidic substrates: 1. Theory, experimental techniques, and effects on separations", *Electrophoresis* **25** (2004) 187–202; doi:10.1002/elps.200305754.
- [35] S. W. Kowalczyk, A. Y. Grosberg, Y. Rabinand and C. Dekker, "Modeling the conductance and DNA blockade of solid-state nanopores", *Nanotechnology* **22** (2011) 315101; doi:10.1088/0957-4484/22/31/315101.
- [36] D. Kozak, W. Anderson, R. Vogel and M. Trau, "Advances in resistive pulse sensors: Devices bridging the void between molecular and microscopic detection", *Nano Today* **6** (2011) 531–545; doi:10.1016/j.nantod.2011.08.012.
- [37] W. J. Lan, D. A. Holden, J. Liu and H. S. White, "Pressure-driven nanoparticle transport across glass membranes containing a conical-shaped nanopore", *J. Phys. Chem. C* **115** (2011) 18445–18452; doi:10.1021/jp204839j.
- [38] W. J. Lan, D. A. Holden, B. Zhang and H. S. White, "Nanoparticle transport in conical-shaped nanopores", *Anal. Chem.* **83** (2011) 3840–3847; doi:10.1021/ac200312n.
- [39] S. Lee, Y. Zhang, H. S. White, C. C. Harrell and C. R. Martin, "Electrophoretic capture and detection of nanoparticles at the opening of a membrane pore using scanning electrochemical microscopy", *Anal. Chem.* **76** (2004) 6108–6115; doi:10.1021/ac049147p.
- [40] Y. Liebes, M. Drozdov, Y. Y. Avital, Y. Kauffmann, H. Rapaport, W. D. Kaplan and N. Ashkenasy, "Reconstructing solid state nanopore shape from electrical measurements", *Appl. Phys. Lett.* **97** (2010) 223105; doi:10.1063/1.3521411.
- [41] M. Low, S. Yu, M. Y. Han and X. Su, "Investigative study of nucleic acid–gold nanoparticle interactions using laser-based techniques, electron microscopy, and resistive pulse sensing with a nanopore", *Aust. J. Chem.* **64** (2011) 1229–1234; doi:10.1071/CH11200.
- [42] M. Platt, G. R. Willmott and G. U. Lee, "Resistive pulse sensing of analyte-induced multi-component rod aggregation using tunable pores", *Small* **8** (2012) 2436–2444; doi:10.1002/smll.201200058.

- [43] Z. Qin, J. Zhe and G. X. Wang, "Effects of particle's off-axis position, shape, orientation and entry position on resistance changes of micro Coulter counting devices", *Meas. Sci. Technol.* **22** (2011) 045804; doi:10.1088/0957-0233/22/4/045804.
- [44] P. Ramírez, P. Y. Apel, J. Cervera and S. Mafé, "Pore structure and function of synthetic nanopores with fixed charges: Tip shape and rectification properties", *Nanotechnology* **19** (2008) 315707; doi:10.1088/0957-4484/19/31/315707.
- [45] C. L. Rice and R. Whitehead, "Electrokinetic flow in a narrow cylindrical capillary", *J. Phys. Chem.* **69** (1965) 4017–4025; doi:10.1021/j100895a062.
- [46] G. S. Roberts, D. Kozak, W. Anderson, M. F. Broom, R. Vogel and M. Trau, "Tunable nano/micropores for particle detection and discrimination: Scanning ion occlusion spectroscopy", *Small* **6** (2010) 2653–2658; doi:10.1002/sml.201001129.
- [47] G. S. Roberts, S. Yu, Q. Zeng, L. C. L. Chan, W. Anderson, A. H. Colby, M. W. Grinstaff, S. Reid and R. Vogel, "Tunable pores for measuring concentrations of synthetic and biological nanoparticle dispersions", *Biosens. Bioelectron.* (2012); doi:10.1016/j.bios.2011.09.040.
- [48] O. A. Saleh and L. L. Sohn, "An artificial nanopore for molecular sensing", *Nano Lett.* **3** (2003) 37–38; doi:10.1021/nl0255202.
- [49] R. A. Sampson, "On Stokes's current function", *Phil. Trans. R. Soc. Lond. A* **182** (1891) 449–518; doi:10.1098/rsta.1891.0012.
- [50] J. G. Santiago, "Electroosmotic flows in microchannels with finite inertial and pressure forces", *Anal. Chem.* **73** (2001) 2353–2365; doi:10.1021/ac0101398.
- [51] R. B. Schoch, J. Han and P. Renaud, "Transport phenomena in nanofluidics", *Rev. Mod. Phys.* **80** (2008) 839–883; doi:10.1103/RevModPhys.80.839.
- [52] L. T. Sexton, L. P. Horne and C. R. Martin, "Developing synthetic conical nanopores for biosensing applications", *Mol. BioSyst.* **3** (2007) 667–685; doi:10.1039/b708725j.
- [53] Z. S. Siwy and M. Davenport, "Making nanopores from nanotubes", *Nat. Nanotech.* **5** (2010) 174–175; doi:10.1038/nnano.2010.33.
- [54] W. R. Smythe, "Flow around the spheroid in a circular tube", *Phys. Fluids* **7** (1964) 633–638; doi:10.1063/1.1711260.
- [55] Y. Song, H. Zhang, C. H. Chon, X. Pan and D. Li, "Nanoparticle detection by microfluidic resistive pulse sensor with a submicron sensing gate and dual detecting channels—two stage differential amplifier", *Sens. Actuators B* **155** (2011) 930–936; doi:10.1016/j.snb.2011.01.004.
- [56] S. J. Sowerby, M. F. Broom and G. B. Petersen, "Dynamically resizable nanometre-scale apertures for molecular sensing", *Sens. Actuators B* **123** (2007) 325–330; doi:10.1016/j.snb.2006.08.03.
- [57] L. J. Steinbock, G. Stober and U. F. Keyser, "Sensing DNA-coatings of microparticles using micropipettes", *Biosens. Bioelectron.* **24** (2009) 2423–2427; doi:10.1016/j.bios.2008.12.026.
- [58] G. Stober, L. J. Steinbock and U. F. Keyser, "Modeling of colloidal transport in capillaries", *J. Appl. Phys.* **105** (2009) 084702; doi:10.1063/1.3095761.
- [59] L. Sun and R. M. Crooks, "Single carbon nanotube membranes: A well-defined model for studying mass transport through nanoporous materials", *J. Am. Chem. Soc.* **122** (2000) 12340–12345; doi:10.1021/ja002429w.
- [60] S. van Dorp, U. F. Keyser, N. H. Dekker, C. Dekker and S. G. Lemay, "Origin of the electrophoretic force on DNA in solid-state nanopores", *Nature Phys.* **5** (2009) 347–351; doi:10.1038/nphys1230.
- [61] R. Vogel, W. Anderson, J. Eldridge, B. Glossop and G. R. Willmott, "A variable pressure method for characterizing nanoparticle surface charge using pore sensors", *Anal. Chem.* **84** (2012) 3125–3132; doi:10.1021/ac2030915.
- [62] R. Vogel, G. R. Willmott, D. Kozak, G. S. Roberts, W. Anderson, L. Groenewegen, B. Glossop, A. Barnett, A. Turner and M. Trau, "Quantitative sizing of nano/microparticles with a tunable elastomeric pore sensor", *Anal. Chem.* **83** (2011) 3499–3506; doi:10.1021/ac200195n.
- [63] G. Wang, B. Zhang, J. R. Wayment, J. M. Harris and H. S. White, "Electrostatic-gated transport in chemically modified glass nanopore electrodes", *J. Am. Chem. Soc.* **128** (2006) 7679–7686; doi:10.1021/ja061357r.
- [64] W. Wang-yi and R. Skalak, "The Stokes flow from half-space into semi-infinite circular cylinder", *Appl. Math. Mech.* **6** (1985) 9–23; doi:10.1007/BF01895679.

- [65] E. W. Washburn, "The dynamics of capillary flow", *Phys. Rev.* **17** (1921) 273–283; doi:10.1103/PhysRev.17.273.
- [66] J. E. Wharton, P. Jin, L. T. Sexton, L. P. Horne, S. A. Sherrill, W. K. Mino and C. R. Martin, "A method for reproducibly preparing synthetic nanopores for resistive-pulse biosensors", *Small* **3** (2007) 1424–1430; doi:10.1002/sml.200700106.
- [67] G. R. Willmott, M. F. Broom, M. L. Jansen, R. M. Young and W. M. Arnold, *Tunable elastomeric pores, in molecular- and nano-tubes* (Springer-Verlag, Berlin, 2011).
- [68] G. R. Willmott, R. Chaturvedi, S. Cummins and L. G. Groenewegen, "Actuation of tunable elastomeric pores: Resistance measurements and finite element modelling", *Exper. Mech.* (2013); doi:10.1007/s11340-013-9795-5.
- [69] G. R. Willmott and P. W. Moore, "Reversible mechanical actuation of elastomeric nanopores", *Nanotechnology* **19** (2008) 475504; doi:10.1088/0957-4484/19/47/475504.
- [70] G. R. Willmott and B. E. T. Parry, "Resistive pulse asymmetry for nanospheres passing through tunable submicron pores", *J. Appl. Phys.* **109** (2011) 094307; doi:10.1063/1.3580283.
- [71] G. R. Willmott, M. Platt and G. U. Lee, "Resistive pulse sensing of magnetic beads and supraparticle structures using tunable pores", *Biomicrofluidics* **6** (2012) 014103; doi:10.1063/1.3673596.
- [72] G. R. Willmott and B. G. Smith, "Comment on 'Modeling the conductance and DNA blockade of solid-state nanopores'", *Nanotechnology* **23** (2012) 088001; doi:10.1088/0957-4484/23/8/088001.
- [73] G. R. Willmott, R. Vogel, S. S. C. Yu, L. G. Groenewegen, G. S. Roberts, D. Kozak, W. Anderson and M. Trau, "Use of tunable nanopore blockade rates to investigate colloidal dispersions", *J. Phys.: Condens. Matter* **22** (2010) 454116; doi:10.1088/0953-8984/22/45/454116.
- [74] G. R. Willmott, S. S. C. Yu and R. Vogel, "Pressure dependence of particle transport through resizable nanopores", *Proceedings of ICONN 2010, Sydney, Australia*; doi:10.1109/ICONN.2010.6045207.
- [75] S. Wu, S. R. Park and X. S. Ling, "Lithography-free formation of nanopores in plastic membranes using laser heating", *Nano Lett.* **6** (2006) 2571–2576; doi:10.1021/nl0619498.